Supplement to: Abundances, emissions and loss processes of the long-lived and potent greenhouse gas octafluorooxolane (octafluorotetrahydrofuran, *c*-C_4F_8O) in the atmosphere

Martin K. Vollmer[1], François Bernard[2,3,4], Blagoj Mitrevski[5], L. Paul Steele[5], Cathy M. Trudinger[5], Stefan Reimann[1], Ray L. Langenfelds[5], Paul B. Krummel[5], Paul J. Fraser[5], David M. Etheridge[5], Marc A. J. Curran[6,7], and James B. Burkholder[2]

[1]Laboratory for Air Pollution and Environmental Technology, Empa, Swiss Federal Laboratories for Materials Science and Technology, Dübendorf, Switzerland
[2]Earth System Research Laboratory, NOAA, National Oceanic and Atmospheric Administration, Boulder, Colorado, USA
[3]Cooperative Institute for Research in Environmental Sciences, University of Colorado, Boulder, Colorado, USA
[4]now at: Institut de Combustion Aérothermique, Réactivité et Environnement, Centre National de la Recherche Scientifique, Observatoire des Science de l'Univers en région Centre, Orléans, France
[5]Climate Science Centre, CSIRO Oceans and Atmosphere, Aspendale, Victoria, Australia
[6]Australian Antarctic Division, Kingston, Tasmania, Australia
[7]Antarctic Climate & Ecosystems Cooperative Research Centre, Hobart, Tasmania, Australia

Correspondence to: Martin K. Vollmer
(martin.vollmer@empa.ch)

S-1 Introduction

The supplement of this article consists of this text file and the following separate tables, saved as ascii files:

Table S1. Infrared absorption spectra.

Table S2. O(^{1}D) reaction rates.

Table S3. Measurement results for archived air samples and in situ observations.

Table S4. Inversion results for archived air samples and in situ observations.

S-2 Analytical details

S-2.1 Infrared absorption spectra

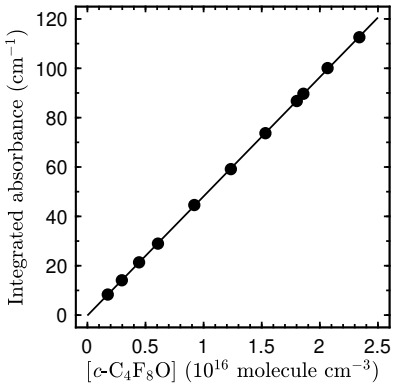

Figure S1. Beer's law plot for the 296 K infrared spectra of octafluorooxolane (c-C_4F_8O) over the wavenumber region 900–1500 cm^{-1}. The line is a linear least-square fit to the data set, forced through the origin. The absorption length was 15 cm.

S-2.2 UV absorption

An example of a measured gas-phase UV spectrum of c-C_4F_8O at 296 K is shown in Fig. S2.

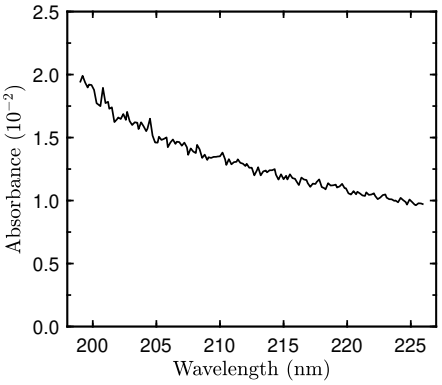

Figure S2. Measured gas-phase UV spectrum at 296 K of the c-C_4F_8O sample used in this study. The c-C_4F_8O concentration was 2.16×10^{19} molecule cm^{-3}. Assuming no absorption from possible sample impurities, the c-C_4F_8O absorption cross section at 210 nm was found to be 6.25×10^{-24} cm^2 molecule^{-1}. As discussed in Section 3.2 of the main text, such a low cross section is susceptible to overestimation due to the presence of impurities in the c-C_4F_8O sample. Therefore, this spectrum was considered as an upper-limit in our lifetime analysis.

S-2.3 O(^{1}D) reaction

Table S5. Summary of the relative rate measurements for the reaction O(^{1}D) + *c*-C_4F_8O at 296 K.

Experiment	Pressure range (Torr)	k_{1a}/k_{2a} [a]	k_{1a} (10^{-12} cm^3 molecule^{-1} s^{-1})[b]
1	312–669	0.287±0.010	0.69
2	100–495	0.175±0.007	0.42
3	101–630	0.167±0.011	0.40

a) 2σ fit precision uncertainty

b) $k_{2a} = 2.41\times10^{-12}$ cm^3 molecule^{-1} s^{-1}.

S-2.4 Medusa GCMS identification and mass spectra

GCMS identification of *c*-C_4F_8O for this work was based on the measurements of the compound in a diluted mixture of known composition. A GS-GasPro main capillary column (0.32 mm ID × 60 m, Agilent Technologies) was used for the main separation and a column of the same type (5 m) was fitted as a precolumn, allowing for a backflushing of late eluting compounds. In the GCMS setup used in this work (Agilent 6890 GC, 5975 MS) the MS was used in scan and selected ion modes. *c*-C_4F_8O elutes at 1408 s, 8 s after iso/normal-perfluorobutanes, 2 s after HFC-134a and 6 s before methyl chloride. It was identified based on the fragments $C_3F_6^+$ (m/z 150) and $C_2F_4^+$ (m/z 100) as a result of the mass fragmentation of the *c*-C_4F_8O molecule. The choice for these ions was based on the mass spectrum measured in this work for *c*-C_4F_8O, to the best of our knowledge the first one published for this compound.

Mass spectra were measured on two instruments and results are given in Table S6. One *c*-C_4F_8O mass spectrum was measured on the Empa laboratory Medusa GCMS (Medusa-20), fitted with a Porabond Q column, using a diluted aliquot of the pure substance (SynQuest Laboratories, Inc., Alachua, Florida, USA, Lot #Q14B-29). The mass spectrum was measured in the range 49–225 mass/charge (m/z). Another mass spectrum was measured on Medusa-9, which is the instrument used for the archived air sample analysis. For this purpose, an aliquot of a diluted mixture of HCP-Carba-04 was combined with a selection of other pure compounds to produce a high-concentration multi-component mixture in synthetic air. Here the measured m/z scan range was chosen as 18–250. The percentages listed in Table S6 are relative to the most abundant fragment, which was chosen as 100 %. These mass spectra were somewhat surprising. Oxygen-containing fragments were only weakly present, $C_2OF_3^+$ being the most abundant of them (3 %), followed by $C_3OF_3^+$ (m/z 109) and $C_3OF_4^+$ (m/z 128) at <1 % compared to the most abundant fragment. Also, the abundant m/z 69, which we interpret as CF_3^+, is suggested to be the result of a rearrangement of atoms during ionization, because a simple break-up of the cyclic structure, which has two fluorines attached to each carbon, could not produce such a fragment. The same line of reasoning applies for m/z 169 ($C_3F_7^+$) and m/z 119 ($C_2F_5^+$), which are also

relatively abundant. We have not found published mass spectra for *c*-C_4F_8O in the literature, with which we could compare our results. Such rearrangements are known for fully fluorinated cyclic fluorocarbons as is shown by Mohler et al. (1952) or on the internet by the National Institute of Standards and Technology (NIST, 2018). For example, for *c*-C_4F_8 (CAS 115-25-3), *c*-C_5F_{10} (CAS 376-77-2), and *c*-C_6F_{12} (CAS 355-68-0) the fragments with m/z 69 (high abundance) and 119 are also both present in their mass spectra. Our own unpublished work also shows that for *c*-C_3F_6 (CAS 931-91-9), the CF_3^+ fragment (m/z 69), is the second-most abundant fragment.

Table S6. Mass spectra for *c*-C_4F_8O based on gas-chromatography Electron-Impact (EI) ionization mass spectrometry (Agilent 5975 MS) for two Medusa-GCMS instruments. The range chosen for Medusa-20 was m/z 49–225, and that for Medusa-9 was 18–250.

	Medusa-20			Medusa-9	
abundance in %	measured m/z	assumed fragment	abundance in %	measured m/z	assumed fragment
100	100	$C_2F_4^+$	100	100	$C_2F_4^+$
38	69	CF_3^+	46	69	CF_3^+
37	150	$C_3F_6^+$	29	150	$C_3F_6^+$
25	169	$C_3F_7^+$	16	169	$C_3F_7^+$
7	131	$C_3F_5^+$	5	50	CF_2^+
5	119	$C_2F_5^+$	5	131	$C_3F_5^+$
5	50	CF_2^+	4	119	$C_2F_5^+$
3	97	$C_2OF_3^+$	3	97	$C_2OF_3^+$

S-2.5 Medusa-GCMS Nonlinearity Experiments

Two different types of nonlinearity tests were performed as part of the archived air analysis. In a first test (volume-non-linearity), variable volumes of the standard E-146S were measured, alternating with measurements of 3 L volume samples of this standard. Within measurement uncertainties, and when volume-corrected, this showed a constant response relative to the standards' injections. However because of the relatively high mole fraction of *c*-C_4F_8O in E-146S ($\sim$500 ppq) and limitations to the instrumental technique, this method did not allow for the complete coverage of the full range measured in our archived air samples (only to $\sim$50 ppq). In a second experiment, a molar non-linearity was determined by a pressure-based dilution of an aliquot of the standard E-146S, which was measured (two measurements per dilution) against the undiluted E-146S each time before it was further diluted in the same canister (4.5 L internally electropolished stainless steel tank, Essex Industries, USA). The canister was immersed in a water bath to thermally stabilize and pressure was allowed to equilibrate after each dilution step. Pressure was accurately measured (pressure gauge CRYSTAL XP2i, Crystal Engineering Corporation, San Luis Obispo, CA, USA). For the dilution, purified synthetic air was used, which was prepared similar to that described by Vollmer et al. (2015) and shown to be free of *c*-C_4F_8O. The measured mole fractions in the diluted sample measurements were compared to the calculated mole fraction and also to the mole fraction of compounds with large peak sizes (CCl_2F_2 and CCl_3F). This test showed linearity within the measurement uncertainties for a tested range covering 500 ppq (upper limit) to the detection limits ($\sim$5 ppq). These tests further showed the absence of blanks, memory effects, nafion drier interferences, or other potential

systematic biases, as the fitted curve of the mole fraction vs. the dilution ratio intersected the origin, and the slope of the fit equaled (within measurement uncertainties) the mole fraction of the E-146S standard. These results are presented in Figure S3, and zoomed into the more relevant range for this analysis, in Figure S4.

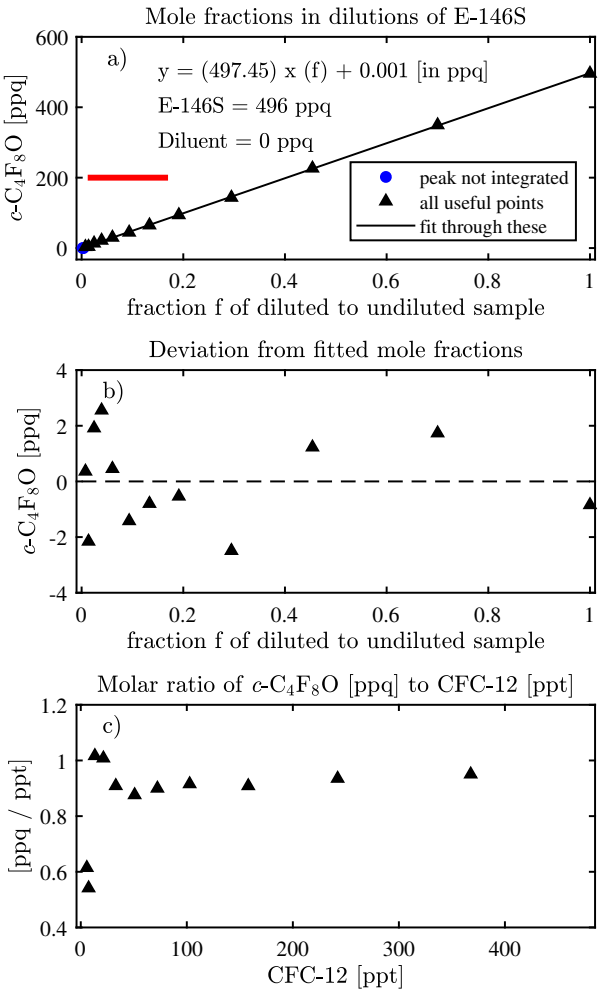

Figure S3. Results of experiments to test for non-linearity of response in measurements of c-C_4F_8O using pressure-based dilutions of an aliquot of the standard E-146S. a) Measured mole fractions as a function of the dilution ratio to E-146S — dilutions were made from an aliquot of E-146S (at f=1.0, from right to left). The slope of the fit agrees well with the mole fraction in the undiluted sample and the f=0 crossing is close to zero. The red bar denotes the mole fraction range of the measured air samples. b) Deviation from fit in a). c) Molar ratio to CFC-12. Mole fractions are given in ppq (parts per quadrillion, fmol mol^{-1}) for c-C_4F_8O and in ppt for CFC-12 (parts per trillion, pmol mol^{-1}). These results suggest a linear system response within the measurement precision and in the range of the measured sample mole fractions.

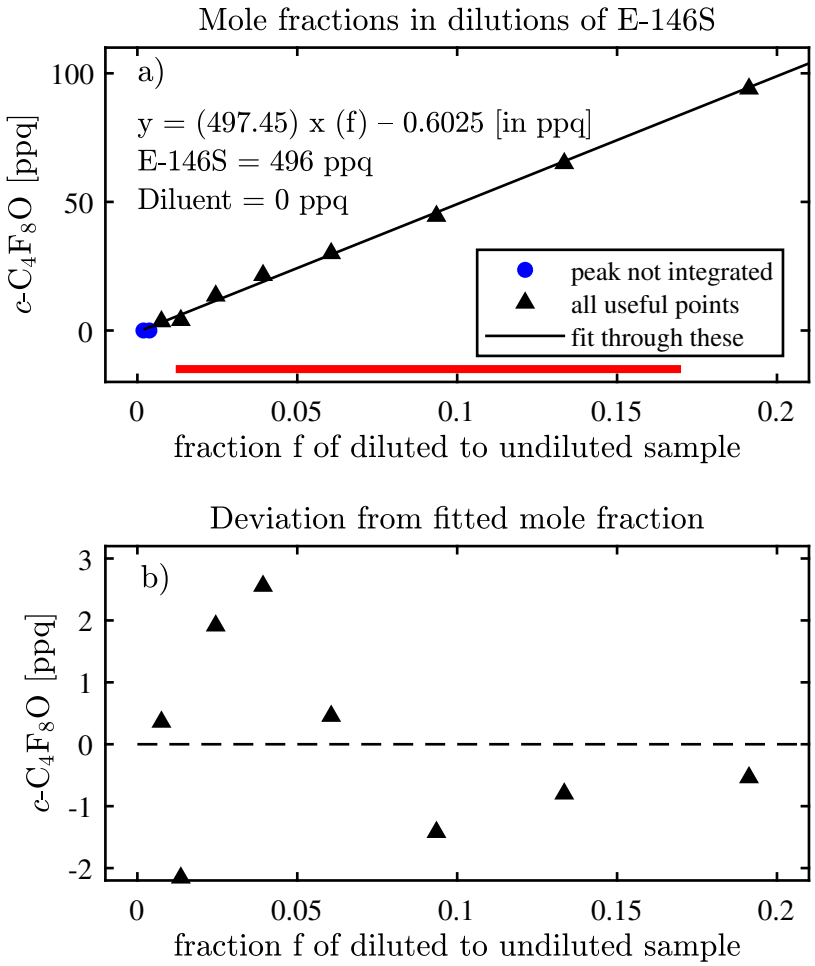

Figure S4. Results of experiments to test for non-linearity of response in measurements of c-C_4F_8O using pressure-based dilutions of an aliquot of the standard E-146S. Same as Figure S3 but for a narrower range of the dilution factor f.

S-2.6 Northern Hemisphere (NH) samples

The Southern Hemisphere Cape Grim Air Archive (CGAA) samples were complemented with a few archived air samples from the NH (see also Table S3). Some of these samples were collected as whole air ambient background samples for original calibration purposes: UAN920470 at Cape Meares, Oregon, most likely cryogenic techniques; T-EMPA-1 and J-187 at La Jolla, California using an oil-free diving compressor (Rix Industries); EG-003 at Jungfraujoch, Switzerland, using cryogenic techniques. H-160 at Mace Head, Ireland, using an oil-free diving compressor. These samples were all collected in internally electropolished stainless steel canisters (Essex Industries, USA). Two samples collected at Dübendorf (DUE161216-D2 and DUE161216) were collected into 6-L internally electropolished cylindrical custom-fabricated containers (LabCommerce, California) using a diaphragm pump (KNF-N-022-ANE, Neuberger), for the specific purpose of this project. These two sam-

ples, and EG-003 and H-160 were shipped from Empa to CSIRO for analysis along with the CGAA samples under the same measurement conditions.

S-2.7 In-situ measurements of c-C_4F_8O at Aspendale

Regular measurements of c-C_4F_8O in ambient air at Aspendale were started in February 2017. These were conducted on a 2-hourly basis where each air measurement is bracketed by standard measurements. The standards used for these measurements were collected as whole air samples at Cape Schanck (Victoria, Australia) using an oil-free diving compressor, and were spiked with small quantities of c-C_4F_8O to better track the mass spectrometer sensitivity. Results are shown in Fig. S5. A few ambient air measurements were also made in late 2016 during the CGAA measurement phase. These were made from 3 L samples (vs. the regular 2 L samples) and show improved precisions compared to the remaining record. The 2-year record shows constant c-C_4F_8O mole fractions within the precisions of the measurements. There is no sign of any pollution events in this record suggesting that there are no significant sources of c-C_4F_8O within the footprint of the site. Furthermore and given the long atmospheric lifetime of the compound, the absence of a significant trend is suggestive of the absence of major global emissions in the last year.

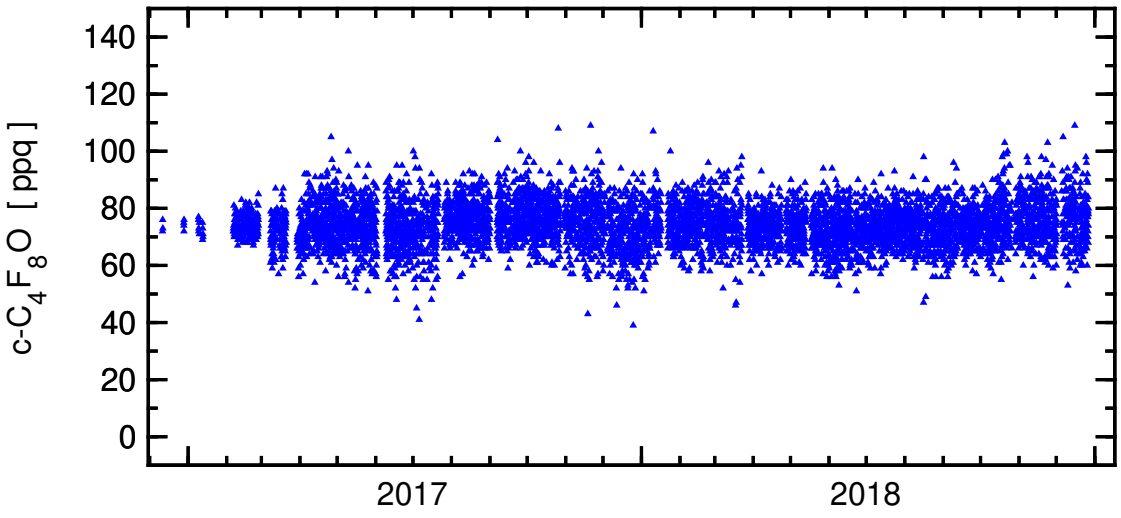

Figure S5. Ambient air measurements of c-C_4F_8O at Aspendale (Victoria, Australia, 38.0°S, 145.1°E). The measurements are expressed as dry air mole fraction in parts-per-quadrillion on the Empa-2013 calibration scale. Results show constant c-C_4F_8O within the precision of the measurement.

S-2.8 Measurements of *c*-C_4F_8O on other instruments

Measurements of *c*-C_4F_8O using the "traditional" AGAGE Medusa-GCMS Porabond Q chromatography column (Miller et al., 2008) revealed some difficulties. We have routinely measured *c*-C_4F_8O in ambient air samples at Jungfraujoch and urban Dübendorf (Switzerland) since late 2012 using Porabond Q columns. However on the columns used in these two Medusa-GCMSs (Medusa-12 and Medusa-20, respectively), *c*-C_4F_8O elutes shortly after *c*-C_4F_8 (PFC-318), normal-C_4F_{10} and iso-C_4F_{10}, and occasionally and also after another unidentified compound, and is negatively influenced by common ion fragments. Integrations of the small *c*-C_4F_8O chromatographic peaks are difficult and error-prone. For this reason we refrain from reporting the >5 year long records at these two stations. However within the uncertainties of the measurements we can report the absence of pollution events over this period indicating the absence of significant *c*-C_4F_8O emissions within the footprints of the two sites.

Larger chromatographic peaks, such as those resulting from measurements of standards spiked with *c*-C_4F_8O, were not negatively influenced by the above-mentioned interference and allowed to maintain and propagate an internally consistent set of calibration standards.

S-3 Diffusivity in the firn model calculations for Aurora Basin North (ABN)

Firn air transport is dominated by molecular diffusivity throughout most of the firn, however it has been shown recently (Buizert and Severinghaus, 2016) that dispersion driven by synoptic scale surface pressure variability (or barometric pumping) dominates mixing in the region of the lower firn known as the lock-in zone. Including lock-in zone dispersion in a firn model has been found to improve the fit to observations in some cases (Buizert et al., 2012; Buizert and Severinghaus, 2016), however it can be difficult to constrain with the available observations at some sites (Trudinger et al., 2013). Isotopic ratios are particularly sensitive to the inclusion of dispersion. The firn model calculations for ABN presented here only considered molecular diffusion and did not include dispersion in the lock-in zone. The CSIRO model is capable of including both, and future studies with the CSIRO firn model will investigate dispersion in the lock-in zone at ABN. The omission of dispersion in the lock-in zone for the *c*-C_4F_8O work is believed to have only made a small difference to the Green's function for the deep firn measurement, within the range of the other uncertainties. As we found that the deep firn measurement did not constrain the timing of the mole fraction or emissions history prior to the archive record anyway, inclusion of dispersion would not change this conclusion.

S-4 Inversion details

The inversion calculation estimates annual *c*-C_4F_8O emissions using the two ABN firn measurements and annual values from a smoothing spline fit (with 50% attenuation at periods of 10 years) to CGAA and Aspendale in situ observations. We calculate the uncertainty in estimated emissions using a bootstrap resampling method, where the inversion is repeated using observations that have been perturbed according to their uncertainty, with the ensemble of firn model parameters to represent firn model uncertainty, a range in the background mole fraction (we use up to 1.0 ppq for *c*-C_4F_8O) and various plausible choices for the

north-south distribution of emissions. The year-to-year uncertainty in annual values from the spline is small because interannual variability has been strongly suppressed by the spline smoothing; we therefore do not independently perturb the annual values from the spline according to their uncertainty, as this leads to unrealistically high variability in the estimated emissions. Instead we independently perturb only the firn measurements, and for the annual means we add values from a temporally-correlated function with periods of around 10 years or more. The function we use is

$$f = \mathrm{p}_1 \times \cos(2\pi(t + \mathrm{p}_2)) + \mathrm{p}_3 \times \cos(4\pi(t + \mathrm{p}_4)) + \mathrm{p}_5 \times \cos(6\pi(t + \mathrm{p}_6))$$

where t is $(\mathrm{year} - 1978)/(2019 - 1978)$ and the parameters p_1–p_6 are random numbers in the range [0,1]. The integral of this function over the period 1978 to 2018 is zero, and the magnitude is less than 1.0 most of the time. The function is scaled to achieve the level of systematic error required, for *c*-C_4F_8O we have chosen a magnitude of 1.0 ppq, representing 2σ. We also perturb all mole fraction data by a constant amount (2σ range of ± 15 %) to incorporate the absolute uncertainty in the measurements, predominantly due to uncertainty in the calibration scale.

In Figure S6 we show the sensitivity of calculated emissions to a number of model choices and inputs, including the regularization parameter α (that weights the sum of year-to-year emission changes relative to the model-data mismatch in the cost function (Trudinger et al., 2016)), calibration uncertainty, diffusion coefficient of *c*-C_4F_8O in air relative to CO_2 in air, and the prior emissions estimate (used only as a starting point for the inversion and not included in the cost function). The preferred values of these inputs are indicated in the legends with the asterisks. The preferred value of α is chosen to allow plausible variations in emissions, but not what seem like unrealistic variations. The range in emissions corresponding to ± 15 % uncertainty in absolute mole fraction is shown by the range in Figure S6b. The diffusion coefficient alters the emissions estimate prior to 1978 when the CGAA begins — low values of the relative diffusion coefficient cause high emissions in the 1950s that are probably unrealistic.

We construct a *c*-C_4F_8O prior history from emissions of perfluorooctane because this compound has similarly low abundances and a long lifetime as for *c*-C_4F_8O. For our standard case, we use perfluorooctane emissions published by Ivy et al. (2012) for the 1980–2010 period with the perfluorooctane 2010 value as a constant value for 2010–2017 and the 1980 value for perfluorooctane for the 1950–1980 period. We also test the sensitivity of our results to a number of other prior histories: a) the standard case doubled, b) the standard case halved, c) the standard case with emissions before 1980 extrapolated back to zero in 1950 and d) a small linearly increasing function (all shown in Fig. S6d). Our analysis shows that the emissions derived for *c*-C_4F_8O are rather insensitive to the choice of the prior, because the prior is used as a starting point for the inversion only, and not as a constraint.

We also tested the sensitivity of inferred global emissions and calculated mole fraction in the high latitude boxes to the specified north-south emissions distribution, and found them to be rather insensitive if most emissions are in the NH (Fig. S7).

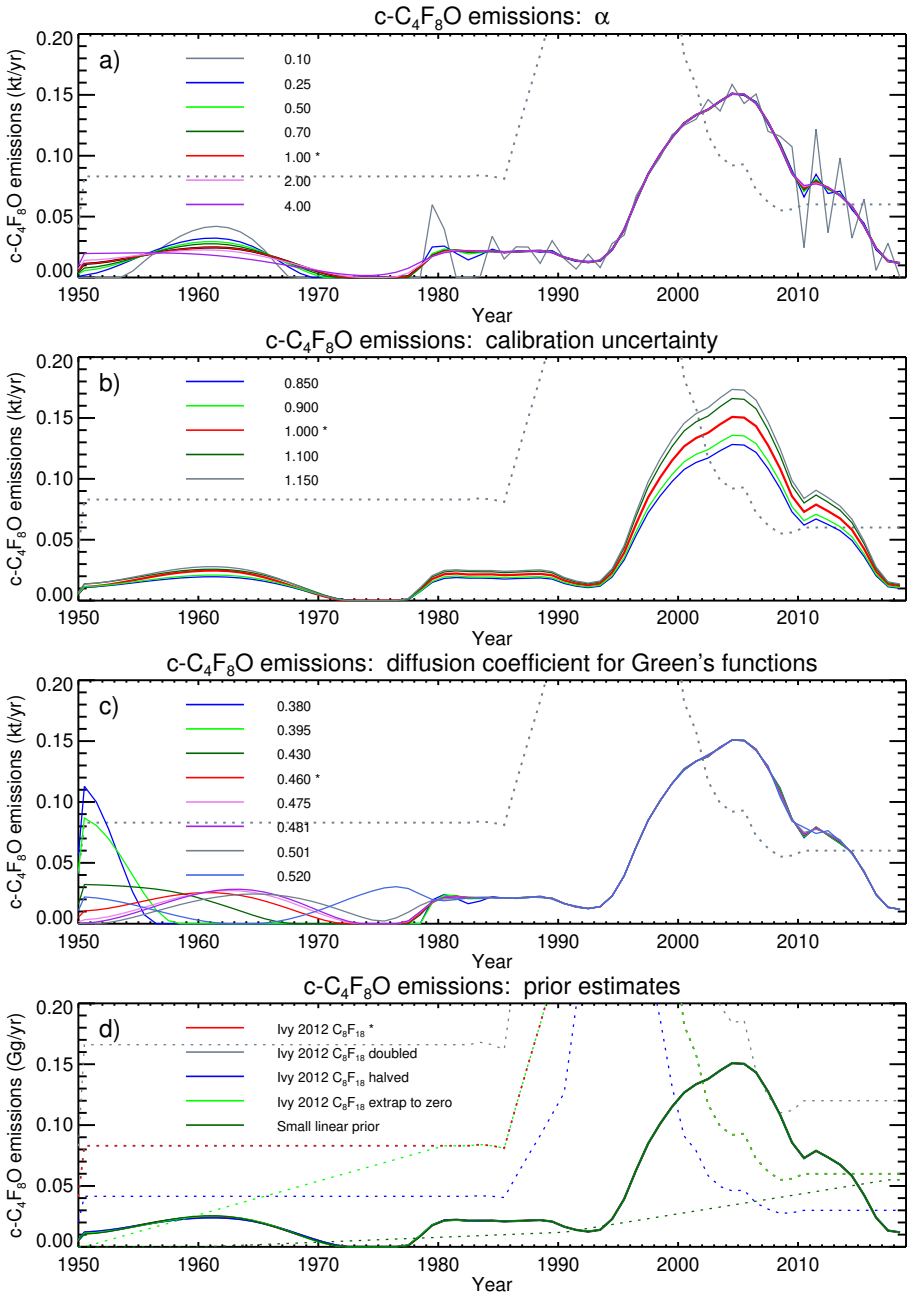

Figure S6. Sensitivities to various parameters in the inversion calculation. a) The parameter α weights the term in the cost function that involves the sum of year-to-year changes in emissions, relative to the model-data mismatch term, b) calibration uncertainty for c-C_4F_8O measurements, that is included in the bootstrap uncertainty calculation, c) diffusion coefficient of c-C_4F_8O relative to the diffusion coefficient of CO_2 that is used in the firn model to calculate the Green's functions, and d) prior emissions used as a starting point for the inversion. In the legend of each panel, the asterisk indicates the choice used in our preferred case.

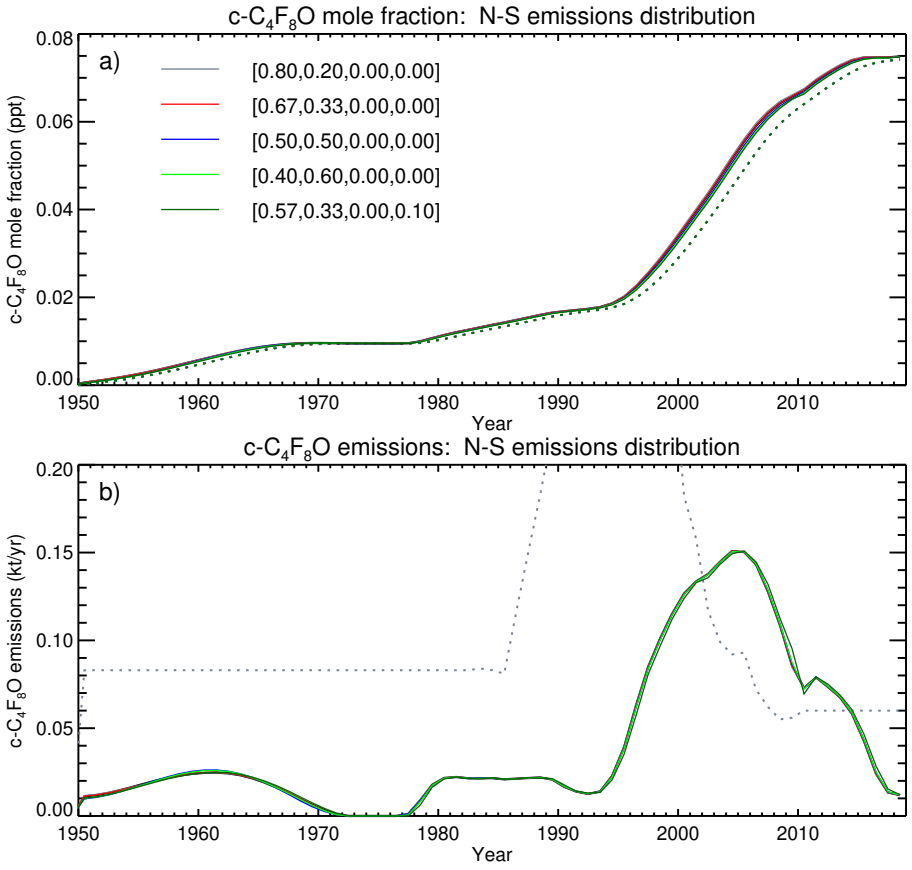

Figure S7. a) Sensitivity of inferred high latitude northern (solid lines) and southern (dashed lines) mole fraction to various proportions of emissions from each semi-hemispheric box in the model. Each case assumes the constant north-south emissions distribution as specified in the legend. b) Inferred global emissions (solid lines) for the cases shown in (a). The dotted line shows the prior emissions.

Figure S8a shows the two ABN measurements of *c*-C_4F_8O in firn, with the modeled depth profile for the inferred emissions. Fig. S8b shows the *c*-C_4F_8O Green's functions from the firn model for the two ABN depths, with colors matching the measurements shown in Fig. S8a. The thick line shows the preferred Green's function, with thin lines showing the ensemble of Green's functions, although they differ little from the preferred function. The shallow ABN sample (from 30.4 m) is shown in blue and contains air mainly from the 2000s up to the firn sampling date in 2013, with a small amount of air from the 1990s and possibly 1980s. The deep ABN sample (from 101.9 m) is shown in green and contains a mix of ages from before 1950 up to at least the 1980s. We know from the CGAA record that atmospheric *c*-C_4F_8O was non-zero in the 1980s, so even if the background level was zero we would expect to see non-zero mole fraction in this sample. We can therefore not determine from the measurements used in this study whether *c*-C_4F_8O is entirely anthropogenic with a zero background, or has a non-zero background level.

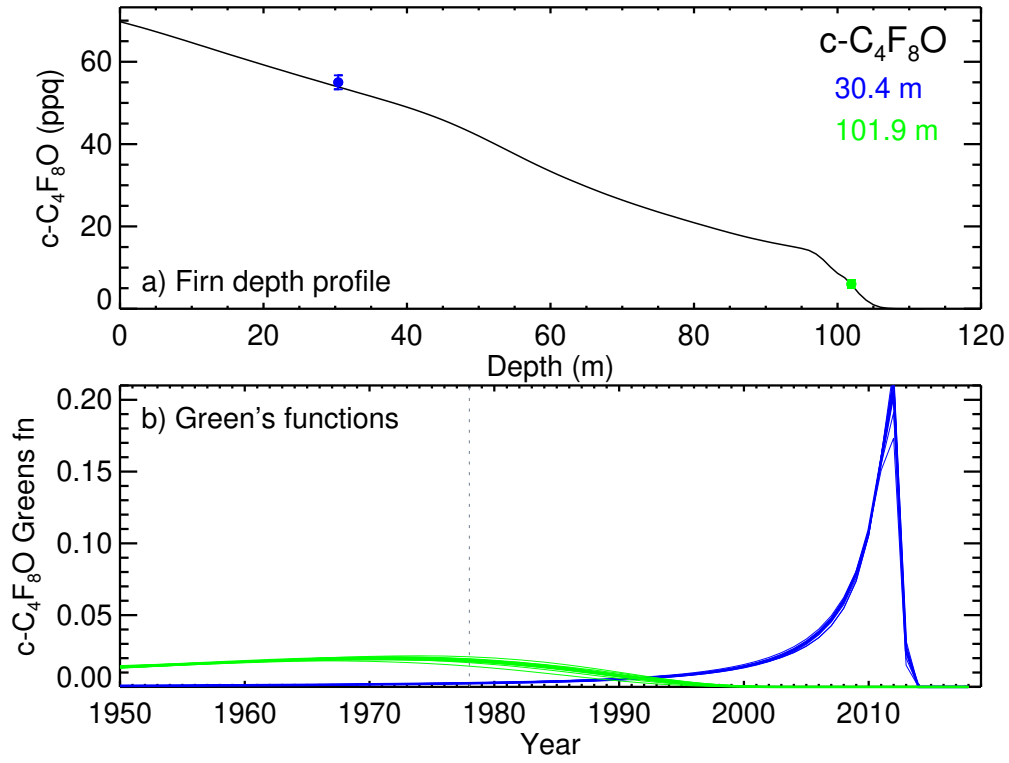

Figure S8. a) Modeled depth profile corresponding to the inferred emissions and b) Green's functions for the two Aurora Basin North (ABN) firn samples, with the sample from 30.4 m shown in blue, and from 101.9 m shown in green.

References

Buizert, C. and Severinghaus, J. P.: Dispersion in deep polar firn driven by synoptic-scale surface pressure variability, The Cryosphere, 10, 2099–2111, doi:10.5194/tc-10-2099-2016, https://www.the-cryosphere.net/10/2099/2016/, 2016.

Buizert, C., Martinerie, P., Petrenko, V. V., Severinghaus, J. P., Trudinger, C. M., Witrant, E., Rosen, J. L., Orsi, A. J., Rubino, M., Etheridge, D. M., Steele, L. P., Hogan, C., Laube, J. C., Sturges, W. T., Levchenko, V. A., Smith, A. M., Levin, I., Conway, T. J., Dlugokencky, E. J., Lang, P. M., Kawamura, K., Jenk, T. M., White, J. W. C., Sowers, T., Schwander, J., and Blunier, T.: Gas transport in firn: multiple-tracer characterisation and model intercomparison for NEEM, Northern Greenland, Atmos. Chem. Phys., 12, 4259–4277, doi:10.5194/acp-12-4259-2012, 2012.

Ivy, D. J., Rigby, M., Baasandorj, M., Burkholder, J. B., and Prinn, R. G.: Global emission estimates and radiative impact of C_4F_{10}, C_5F_{12}, C_6F_{14}, C_7F_{16} and C_8F_{18}, Atmos. Chem. Phys., 12, 7635–7645, doi:10.5194/acp-12-7635-2012, 2012.

Miller, B. R., Weiss, R. F., Salameh, P. K., Tanhua, T., Greally, B. R., Mühle, J., and Simmonds, P. G.: Medusa: A sample preconcentration and GC/MS detector system for in situ measurements of atmospheric trace halocarbons, hydrocarbons, and sulfur compounds, Anal. Chem., 80, 1536–1545, doi:10.1021/ac702084k, 2008.

Mohler, F. L., Dibeler, V. H., and Reese, R. M.: Mass spectra of fluorocarbons, J. Res. Nat. Bur. Stand., 49, 343–347, 1952.

NIST: NIST Chemistry WebBook, SRD 69, https://webbook.nist.gov/chemistry, last accessed 16 May 2018, 2018.

Trudinger, C. M., Enting, I. G., Rayner, P. J., Etheridge, D. M., Buizert, C., Rubino, M., Krummel, P. B., and Blunier, T.: How well do different tracers constrain the firn diffusivity profile?, Atmos. Chem. Phys., 13, doi:10.5194/acp-13-1485-2013, 2013.

Trudinger, C. M., Fraser, P. J., Etheridge, D. M., Sturges, W. T., Vollmer, M. K., Rigby, M., Martinierie, P., Mühle, J. Worton, D. R., Krummel, P. B., Steele, L. P., Miller, B. R., Laube, J., Mani, F., Rayner, P. J., Harth, C. M., Witrant, E., Blunier, T., Schwander, J., O'Doherty, S., and Battle, M.: Atmospheric abundance and global emissions of perfluorocarbons CF_4, C_2F_6 and C_3F_8 since 1800 inferred from ice core, firn, air archive and in situ measurements, Atmos. Chem. Phys., 16, 11 733–11 754, doi:10.5194/acp-16-11733-2016, 2016.

Vollmer, M. K., Rhee, T. S., Rigby, M., Hofstetter, D., Hill, M., Schoenenberger, F., and Reimann, S.: Modern inhalation anesthetics: Potent greenhouse gases in the global atmosphere, Geophys. Res. Lett., 42, 1606–1611, doi:10.1002/2014GL062785, 2015.